Oxygen decreases and variability in the eastern equatorial Pacific

Rena Czeschel,[1] Lothar Stramma,[1] and Gregory C. Johnson[2]

Received 14 March 2012; revised 2 October 2012; accepted 3 October 2012; published 17 November 2012.

[1] Observations indicate increasingly large and strong oxygen minimum zones (OMZs) in the tropical Pacific over recent decades. Here we report on oxygen decreases and variability within the eastern equatorial Pacific OMZ. We construct time series from historical and profiling float oxygen data and analyze data from repeat hydrographic sections at 110°W and 85°50′W. Historical data are quite sparse for constructing oxygen time series, but floats with oxygen sensors prove to be good tools to fill measurement gaps in later parts of these time series. In the region just south of the equator a time series over the last 34 years reveals that oxygen decreases from 200 to 700 m at a rate between 0.50 and 0.83 μmol kg^{-1} yr^{-1}. This strong decrease seems to be related to changes in the Pacific Decadal Oscillation (PDO). Oscillations on shorter time scales (e.g., an El Niño signal in the upper 350 m) are superimposed upon this trend. In the section data, a general trend of decreasing oxygen is present below the surface layer. While velocity differences appear related to oxygen differences in the equatorial channel, there is less correlation elsewhere. Contrasting with long-term trend computations, the trends derived from two repeat sections are obscured by the influence of seasonal and longer-term variability. Multidecadal variability (e.g., PDO) has the strongest influence on long-term trends, while El Niño, isopycnal heave, current variability, seasonal cycles, and temperature changes are less important.

Citation: Czeschel, R., L. Stramma, and G. C. Johnson (2012), Oxygen decreases and variability in the eastern equatorial Pacific, *J. Geophys. Res.*, *117*, C11019, doi:10.1029/2012JC008043.

1. Introduction

[2] Layers with particularly low oxygen concentrations, or oxygen minimum zones (OMZs), are located in the eastern tropical oceans at depths of 100–900 m [e.g., *Karstensen et al.*, 2008]. Century-long integrations of many biogeochemical climate models under global warming conditions predict an overall decline in oceanic dissolved oxygen (O_2) concentration and expansion of the middepth OMZs [*Bopp et al.*, 2002; *Oschlies et al.*, 2008]. However, some models, such as the Geophysical Fluid Dynamics Laboratory's Earth System Model 2.1, do not show an increase in the volume of suboxic waters [*Gnanadesikan et al.*, 2012]. Predicted oxygen changes in the thermocline waters result largely from solubility changes in the upstream source waters [*Matear and Hirst*, 2003], whereas model results reveal physical processes of ventilation and circulation to be the dominant factor of oxygen variability in the lower ventilated thermocline [*Deutsch et al.*, 2006]. Changes in deeper waters mainly result from decreased ocean circulation coupled with ongoing oxygen consumption by remineralization of sinking particulate organic matter [*Matear and Hirst*, 2003].

[3] In the eastern tropical Pacific, eastward zonal currents [e.g., *Kessler*, 2006] could be important in resupplying oxygen to the OMZs [*Stramma et al.*, 2010a]. The most prominent eastward current with a subpycnocline expression is the Equatorial Undercurrent (EUC), which flows eastward along the equator across the entire Pacific [*Johnson et al.*, 2002]. Eastward surface-intensified currents include the weak South Equatorial Countercurrent (SECC), mainly observed in the western basin, and the North Equatorial Countercurrent (NECC), also prominent in the eastern basin (Figure 1). The Pacific subsurface countercurrents (SCCs, also known as Tsuchiya jets [*Tsuchiya*, 1975]) are narrow eastward currents that bracket the equator just below the equatorial thermocline. The northern SCC (NSCC) and the southern SCC (SSCC) start around ±3° from the equator in the western Pacific, then gradually diverge and shoal to the east, with cores around ±6° from the equator and 150 m below the surface by 110°W [*Rowe et al.*, 2000]. At about ±2° from the equator from 500 to 1500 m depth weaker eastward current extrema exist [*Firing et al.*, 1998]: the North and South Intermediate Countercurrents (NICC, SICC). The North Equatorial Current (NEC) and the South Equatorial Current (SEC) are westward surface-intensified currents. A northern branch of the latter is often observed north of the equator. At middepth a westward North Equatorial Intermediate Current

[1]GEOMAR, Helmholtz Centre for Ocean Research Kiel, Kiel, Germany.
[2]Pacific Marine Environmental Laboratory, NOAA, Seattle, Washington, USA.

Corresponding author: R. Czeschel, GEOMAR, Helmholtz Centre for Ocean Research Kiel, Düsternbrooker Weg 20, DE-24105 Kiel, Germany. (rczeschel@geomar.de)

0148-0227/12/2012JC008043

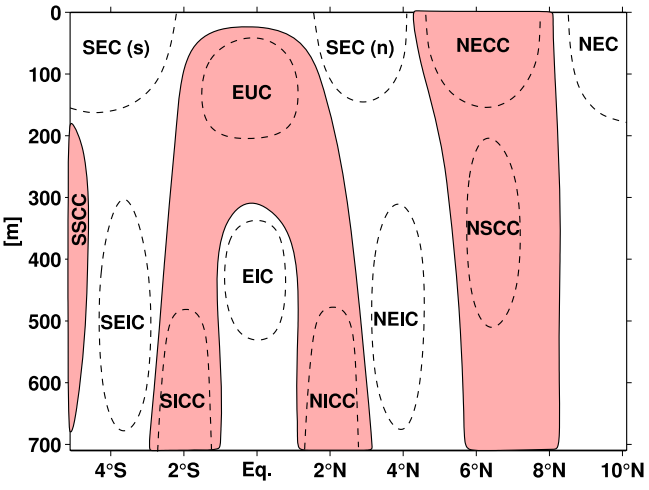

Figure 1. Schematic of zonal currents in the eastern equatorial Pacific. Their locations and strengths will vary in synoptic surveys. For current names, please refer to the text. Pink areas indicate eastward flow. Current cores are indicated by dashed lines.

(NEIC) and a South Equatorial Intermediate Current (SEIC) centered around 500 m and 3° from the equator are observed [*Firing et al.*, 1998]. A westward Equatorial Intermediate Current (EIC) is found below the EUC, especially in the western Pacific [*Johnson et al.*, 2002]. Investigation of the supply paths of oxygen-rich water to the OMZs of the eastern North and South Pacific via zonal tropical currents demonstrated that eastward flows there were about 10–50 μmol kg^{-1} oxygen richer than the westward current bands [*Stramma et al.*, 2010a].

[4] The Galapagos Islands at and south of the equator at 90°W–92°W are a topographic barrier within the eastern Pacific OMZ for both the EUC and the westward flowing SEC [*Eden and Timmermann*, 2004] and are spanned by sections analyzed here, influencing our findings. Early observations described the EUC flowing around the northern side of the Galapagos Islands [*Pak and Zaneveld*, 1973] and as denser and deeper east of the Galapagos [*Knauss*, 1966]. Modeling studies similar to *Eden and Timmermann* [2004] have since been conducted where the islands were treated differently, leading to conflicting results [*Karnauskas et al.*, 2007; *Cravatte et al.*, 2007]. *Karnauskas et al.* [2010] used the available data and model results to describe the interaction between the EUC and the Galapagos Islands but state that the nature of the EUC-like flow at ~85°W, sparsely sampled compared to areas to the west regularly visited by Tropical Atmosphere Ocean (TAO) project cruises, remains a challenging mystery.

[5] Oxygen levels in the tropical Pacific OMZs appear to be decreasing, and the OMZ expanding. In 10° × 10° areas of the tropical Pacific Ocean centered at the equator at 170°W and 110°W oxygen trends up to −0.2 μmol kg^{-1} yr^{-1} were observed over the last 50 years [*Stramma et al.*, 2008]. Smaller boxes between 3°N and 3°S at 170°W, 140°W, 110°W, and 95°W showed oxygen content decreasing as rapidly as −0.55 μmol kg^{-1} yr^{-1} for a 200–700 m layer over the last 30 years, with similar trends for a density layer spanning roughly these depths [*Stramma et al.*, 2010a]. A comparison of the two time periods 1960–1974 and 1990–2008 over 200–700 m showed a general decreasing oxygen trend for the equatorial and tropical Pacific [*Stramma et al.*, 2010b]. These results cover only the long-term trends, with short-term variations unresolved.

[6] Decreasing O_2 concentrations might have dramatic consequences for microbial and chemical cycling of nutrients and entire open ocean ecosystems. For example, shoaling of the tropical OMZ restricts the distribution of tropical pelagic fishes by compressing their habitat within the oxygenated surface layer [*Prince and Goodyear*, 2006].

[7] Here we use historical oxygen data, float-derived oxygen values, and data from two repeat sections to investigate trends in oxygen within the eastern equatorial Pacific OMZs in light of multidecadal, seasonal, and El Niño signatures in oxygen there. We use this information to investigate the ability of section comparisons to describe the oxygen trends.

2. Data

[8] Historical quality-controlled hydrographic data from the HydroBase2 data set [*Curry*, 2008] available as of October 2008 are used for studying the oxygen distribution and its changes in the tropical Pacific. HydroBase data are drawn from the World Ocean Database 2001 [e.g., *Boyer et al.*, 2006] and some specific programs, e.g., the World Ocean Circulation Experiment (WOCE). The data set is augmented with oxygen profiles from the TAO data set (http://www.pmel.noaa/tao/) and with additional recently collected data sets in the eastern tropical Pacific [*Stramma et al.*, 2010b]. Along 110°W and 85°50′W (Figure 2 and Table 1), oxygen distributions from the WOCE period are compared with those from more recent surveys, revealing depth-dependent oxygen changes versus latitude across the equator. Finally, data from four floats with oxygen sensors deployed in February 2009 along 85°50′W [*Czeschel et al.*, 2011] are used to extend time series of historical oxygen measurements.

[9] WOCE section P18 (Table 1) is used only north of 5°S, where it lies along 110°W. Conductivity-temperature-depth (CTD) instrument and oxygen sample data were collected and a lowered Acoustic Doppler Current Profiler (ADCP)

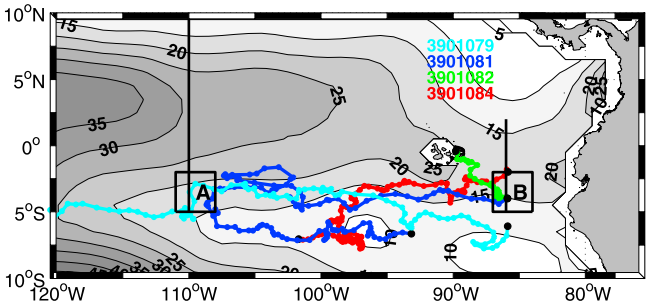

Figure 2. Mean climatological oxygen distribution (shaded contours, μmol kg^{-1}) at 400 m depth from WOA05 [*Boyer et al.*, 2006] with WMO numbers and trajectories (in color) of the five floats which crossed the analyzed boxes A and B (black boxes) between February 2009 and May 2012. The portions of the CTD sections used here along 110°W and 85°50′W are indicated (solid lines). Note the Galapagos Islands near the equator and 90°W–92°W.

Table 1. Details of Sections and Floats Used Here Including Section or WMO Numbers, Ship Names, Section Locations or Deployment Positions, and the Oceanic Nino Indices (ONIs) for the Times of the Sections

WOCE Ship Cruises				
Section Number	Ship	Section	Date	ONI
P18	R/V *Discoverer*	110°W, 5°S–10°N	10–19 Apr 1994	0.4
P18	R/V *Ronald H. Brown*	110°W, 10°N–5°S	24 Dec 2007 to 2 Jan 2008	−1.3
P19	R/V *Knorr*	85°50'W, 5°S–2°N	27 Mar to 1 Apr 1993	0.6
P19	R/V *Meteor*	85°50′W, 5°S–2°N	9–14 Feb 2009	−0.7
Float Deployments				
WMO Number	Ship	Deployment Position	Deployment Date	
3901079	R/V *Meteor*	85°50.00′W, 6°0.01′S	9 Feb 2009	
3901081	R/V *Meteor*	85°50.03′W, 4°0.10′S	10 Feb 2009	
3901082	R/V *Meteor*	85°50.03′W, 4°0.10′S	10 Feb 2009	
3901084	R/V *Meteor*	85°50.03′W, 2°0.21'S	11 Feb 2009	

was attached to the CTD to measure full-depth velocity during this cruise. The cruise proceeded northward, crossing the equator on 13 April 1994. The Oceanic Niño Index (ONI, 3 month running mean SST anomaly for 5°N–5°S, 120°W–170°W) for April 1994 was 0.4. In December 2007 and January 2008 this section was repeated with shipboard ADCP, a CTD, and bottle oxygen samples on the NOAA R/V *Ronald H. Brown* (Table 1). As most of the stations used here were carried out in December 2007, we will call this section the December 2007 section. The ONI for December 2007 was −1.3; hence, the latter cruise was during a La Niña.

[10] The WOCE section P19 (Table 1) was occupied on the R/V *Knorr* from February to April 1993. This section runs along 85°50′W in the equatorial Pacific [*Tsuchiya and Talley*, 1998]. The shipboard ADCP sampling reached a maximum depth of 493 m. Lowered ADCP data were collected only north of 5°S and are used here to extend the vertical range of shipboard ADCP data. The cruise proceeded northward and the northernmost station used here, at 2°N, was taken on 1 April; hence, we call this section the March 1993 section. The ONI was 0.6 for March 1993. The CTD stations from this section were repeated in February 2009. The ONI for February 2009 was −0.7. As for 110°W, the later cruise had a lower ONI than the earlier survey. The shipboard ADCP in February 2009 sampled from the bottom of the ship's hull to 700 m depth. As velocity and hydrographic data have different spatial resolution, the data sets for both sections were first interpolated with objective analysis to a common grid of 0.2° × 10 m.

[11] Ten profiling floats with Aanderaa oxygen sensors were deployed from 2 to 11 February 2009 along the 85°50′W section, in pairs at 10°S, 8°S, 6°S, 4°S, and 2°S. One of each pair had a parking depth of 1000 dbar and the other 400 dbar. All had 10 day surfacing intervals, and all began their mission with a deep profile. The 400 dbar parking depth float deployed at 2°S had pressure sensor problems, and its data are not used here. Four of the deployed floats crossed the boxes used here, and their data through 27 May 2012 are used in oxygen time series (Figure 2 and Table 1).

[12] The CTD oxygen profiles were calibrated by chemical Winkler titrations of bottle oxygen samples. Each Aanderaa oxygen sensor was calibrated by comparing the first float profile with the ship-based CTD-oxygen cast colocated most closely in time and space. Two-point calibrations were applied using the areas of maximum saturation at the near-surface and minimum saturation in the oxygen minimum layer. The calibrated dissolved O_2 concentration was then corrected for salinity and pressure effects using the float pressure and salinity readings (Aanderaa Manual, http://www.aadi.no). The window to transmit oxygen B Phase data by the float hit its limit at very low oxygen values, so the floats did not resolve the lowest oxygen values. CTD-oxygen profiles measured during the float deployment and used for float calibration reveal minimum oxygen values of 3.1 μmol kg^{-1}. These values are up to 2.2 μmol kg^{-1} lower than the minimum oxygen values measured by the floats during the same time and location, so the mean float oxygen data might slightly overestimate the real mean oxygen value.

[13] To investigate trends and seasonal oxygen change, we use the quality-controlled historical data from the HydroBase2 data set, recent data from four profiling floats, and ship-based CTD data at the float deployment positions to construct time series of the annual mean O_2 at various depths averaged yearly within two near-equatorial boxes south of the EUC (A, 108°W–111°W, 5°S–2°S; B, 84°W–87°W, 5°S–2°S). The HydroBase2 data undergo a battery of checks to identify and remove unrealistic points, including visual inspection of property profiles as a function of depth and potential temperature (θ). *Johnson et al.* [2001a] analyzed θ-O_2 differences of cruises where they crossed each other and made relatively small adjustments as a result. For the sections at 110°W and 86°W the oxygen adjustments are 1.0101 at 86°W and 1.0119 at 110°W, negligible compared to the trends we find. We delimit boxes A and B to encompass a wide distribution of data from all decades. However, they cover a smaller area than those used in earlier Pacific investigations [*Stramma et al.*, 2008, 2010a], reducing the confounding influence of geographical oxygen variations. Both WOCE sections cross these boxes and float profiles are in their midst.

[14] Oxygen profiles with a vertical gap in sampling exceeding 100 m in the study depth range are discarded. With this filter applied, almost no profiles covering the upper 700 m before 1976 remain, so the trends are computed for the period following 1976. Despite the limited number of measurements, we investigate seasonal signals by subsampling the data in 3 month seasons and computing long-term trends

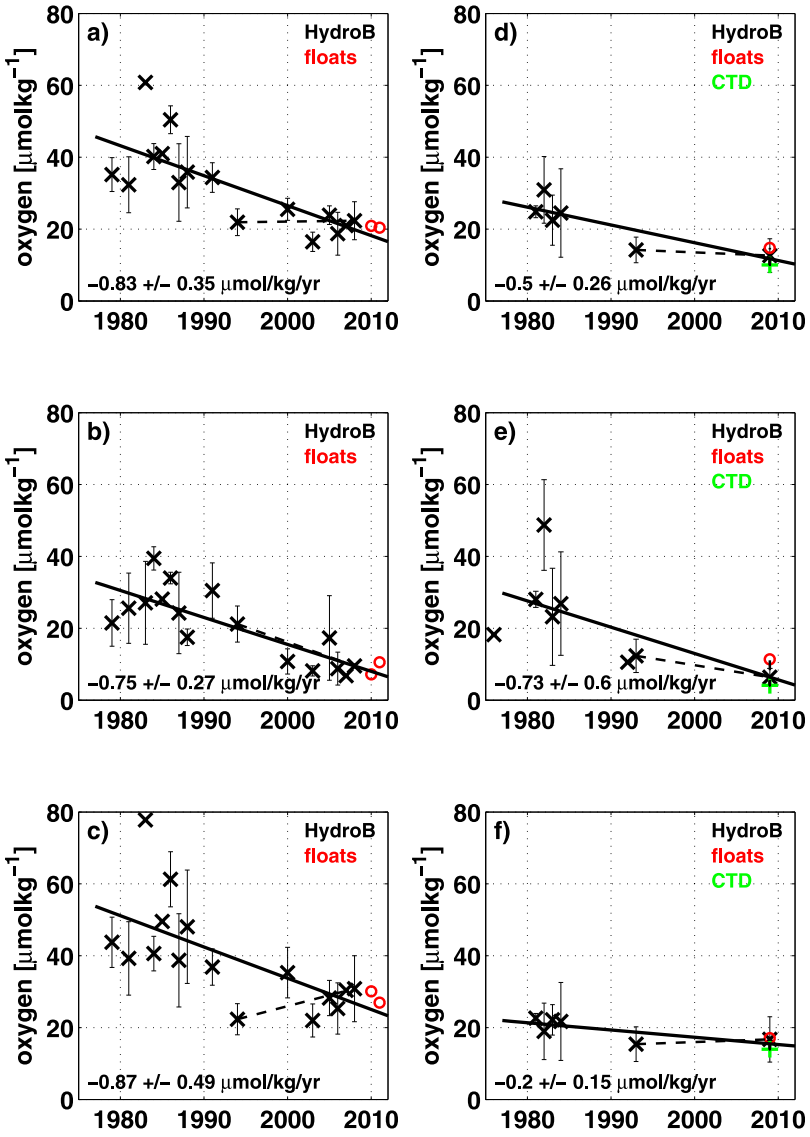

Figure 3. Time series of annual mean (black crosses) O_2 concentrations (μmol kg^{-1}) and standard deviations (error bars) from historical data since 1976, float data (red circles), and CTD data at float deployment locations (green pluses) with linear fits (solid lines) for different depth layers. Analyzed boxes (see Figure 2) are bounded by (a–c) 5°S–2°S, 108°W–111°W and (d–f) 5°S–2°S, 84°W–87°W. Layer depths are 200–700 m (Figures 3a and 3d), 200–400 m (Figures 3b and 3e), and 400–700 m (Figures 3c and 3f). Temporal oxygen trends with 95% confidence intervals are included in each frame. The data from the two pairs of sections (see Figure 8) are connected by dashed lines.

for each of those seasons. To reduce the influence of geographical changes in oxygen, we use 3° × 3° areas.

3. OMZ Changes

[15] As noted above, here we investigate OMZ trends and variability in time series. This investigation is followed by an analysis of oxygen changes and fluxes in hydrographic sections, shedding light on the ability of section comparisons and flux estimates to describe oxygen trends in the OMZ.

3.1. Time Series

[16] To investigate trends and seasonal oxygen changes, time series are constructed within two near-equatorial boxes south of the EUC (A, 108°W–111°W, 5°S–2°S; B, 84°W–87°W, 5°S–2°S). For a data quality check, time series for the upper 20 m depth are verified to be consistent with the saturated values expected at most locations and times in the surface ocean. Time series for the surface ocean do not show a trend for the last 34 years in both boxes south of the EUC, leading to the assumption that the oxygen data used in the deeper part of the ocean are free from large observational biases. Observations before the mid-1990s show more year-to-year variability than more recent data (Figure 3), perhaps owing to larger random measurement noise in earlier bottle data. In addition to oxygen trends, temperature trends are computed to investigate possible relations. If oxygen changes are partly caused by the influence of temperature

Table 2. Temporal Oxygen and Temperature Trends and Their 95% Confidence Intervals With Percentages of the Total Variance Accounted for by Those Oxygen Trends and the Degrees of Freedom (DOF)[a]

Area/Depth Layer (m)	Oxygen Trend/Confidence (μmol kg^{-1} yr^{-1})	Variance	DOF	Temperature Trend/Confidence (°C yr^{-1})
A/200–700	-0.83 ± 0.35	61%	16	0.0023 ± 0.0071
A/200–400	-0.75 ± 0.27	69%	16	-0.0001 ± 0.0071
A/400–700	-0.87 ± 0.49	47%	16	0.005 ± 0.008
B/200–700	-0.50 ± 0.26	78%	6	-0.0078 ± 0.019
B/200–400	-0.73 ± 0.60	56%	8	-0.020 ± 0.022
B/400–700	-0.20 ± 0.15	26%	6	-0.0002 ± 0.015

[a]From linear fits for boxes A (5°S–2°S, 108°W–111°W, time period 1979–2011) and B (5°S–2°S, 84°W–87°W, time period 1976–2009) over three depth layers (Figure 3).

changes on oxygen solubility, temperature increases are expected where oxygen decreases.

[17] Linear trends and their 95% confidence interval [e.g., *Wunsch*, 1996] are computed using annual averages of the profiles linearly interpolated to standard vertical levels. Degrees of freedom for the confidence intervals are determined using integral time scales. These are estimated as twice the maximum of the integrated lagged autocorrelation of the residuals from the trends [e.g., *von Storch and Zwiers*, 1999]. All time series show a significant oxygen decrease for the last 34 years (Figure 3), with trends significantly different from zero at 95% confidence (Table 2). The strongest trend (-0.87 ± 0.49 μmol kg^{-1} yr^{-1}) is in the lower layer of the western part of the OMZ from 400 to 700 m depth (Figure 3c). The deeper layers also show the strongest temperature increase in this area with a positive trend of 0.005 ± 0.008°C yr^{-1} (Table 2). For the 200–400 m layer the temperature trend is negative, but not statistically different from zero. As the oxygen trend in this layer is negative, the observed oxygen trend does not appear to be overly influenced by the local temperature trend.

[18] In the eastern part of the OMZ (box B) the decreasing trend in oxygen is strongest (-0.73 ± 0.6 μmol kg^{-1} yr^{-1}) in the upper OMZ layer between 200 and 400 m (Figure 3e), consistent with the overall, somewhat weaker, decrease of oxygen in the upper 400 m shown along the 85°50′W sections between 1993 and 2009 (see below). In this area the temperature reveals a decrease with the strongest trend of -0.020 ± 0.022°C yr^{-1}, also in the upper layer (Table 2). This pattern might be related to a stronger variability of the supply paths of the upper OMZ: the EUC and SSCC. As for all three computed layers (Table 2), both temperature and oxygen trends are negative, suggesting again that the oxygen trends do not result from temperature-related oxygen solubility changes.

[19] The O_2 trends might be influenced by variability on different time scales. A well-known large spatial-scale long time scale mode of Pacific variability is the Pacific Decadal Oscillation (PDO). The PDO was low between about 1960 and 1975 and high between about 1976 and 1998 [*Deser et al.*, 2010]. Changes in the PDO resulted in higher oxygen off California in the 1980s and 1990s and lower oxygen in the 1960s and since 2000 [*Deutsch et al.*, 2011]. A weaker upwelling and a shallower thermocline in the late 1980s is related to these changes [*Chavez et al.*, 2003]. Our measurement period covers the PDO-related decrease in oxygen and the O_2 trend should be biased high compared to a trend starting in the 1960s. PDO-related near surface temperature trends should decrease more strongly since the mid-1970s compared to the trends since the 1960s.

[20] For the larger region of 5°S–5°N, 115°W–105°W, *Stramma et al.* [2008] used a different approach by combining first all available data in each year into a mean annual profile. They then computed a trend of -0.13 μmol kg^{-1} yr^{-1} since 1960 for 300–700 m. This trend increases to -0.54 μmol kg^{-1} yr^{-1} (by about 400%) using data from the same area but only from 1979 to 2012 for 300–700 m, or -0.70 μmol kg^{-1} yr^{-1} for 200–700 m (Table 3). This larger region includes the smaller area used here in box A, which has an O_2 trend of -0.83 μmol kg^{-1} yr^{-1} for the 200–700 m layer. The temperature trends result in a decrease of -0.0017 ± 0.0092°C yr^{-1} since 1960 and increasing temperature of 0.0015 ± 0.0069°C yr^{-1} when the trend is calculated since 1979 for the area 5°S–5°N, 115°W–105°W (Table 3). However, for the smaller area 3°S–3°N, 115°W–105°W the temperature trends reverse when starting from 1960 versus starting from 1975. All temperature trends are not significantly different from zero at 95% confidence. These results show that oxygen trends are not strongly influenced by the temperature trends nor are they related to the surface layer PDO-related temperature changes.

[21] The O_2 results show that multidecadal variability, probably associated with the PDO, has a strong influence when computing the trend since 1960 instead of 1979.

Table 3. Temporal Oxygen and Temperature Trends and Their 95% Confidence Intervals[a]

Time Period	Area	Depth Layer (m)	Oxygen Trend/Confidence (μmol kg^{-1} yr^{-1})	Temperature Trend/Confidence (°C yr^{-1})
Since 1960	5°S–5°N, 105°–115°W	300–700	-0.13 [*Stramma et al.*, 2008]	-0.0017 ± 0.0092
Since 1979	5°S–5°N, 105°–115°W	300–700	-0.54 ± 0.19	0.0015 ± 0.0069
Since 1979	5°S–5°N, 105°–115°W	200–700	-0.70 ± 0.20	0.0012 ± 0.0065
Since 1960	3°S–3°N, 105°–115°W	200–700	-0.23 ± 0.32	0.0022 ± 0.0041
Since 1975	3°S–3°N, 105°–115°W	200–700	-0.49 ± 0.24 [*Stramma et al.*, 2010a]	-0.0003 ± 0.0073

[a]From linear fits for box 105°W–115°W, 5°S–5°S and 3°S–3°S, respectively, for different time periods and over two depth layers.

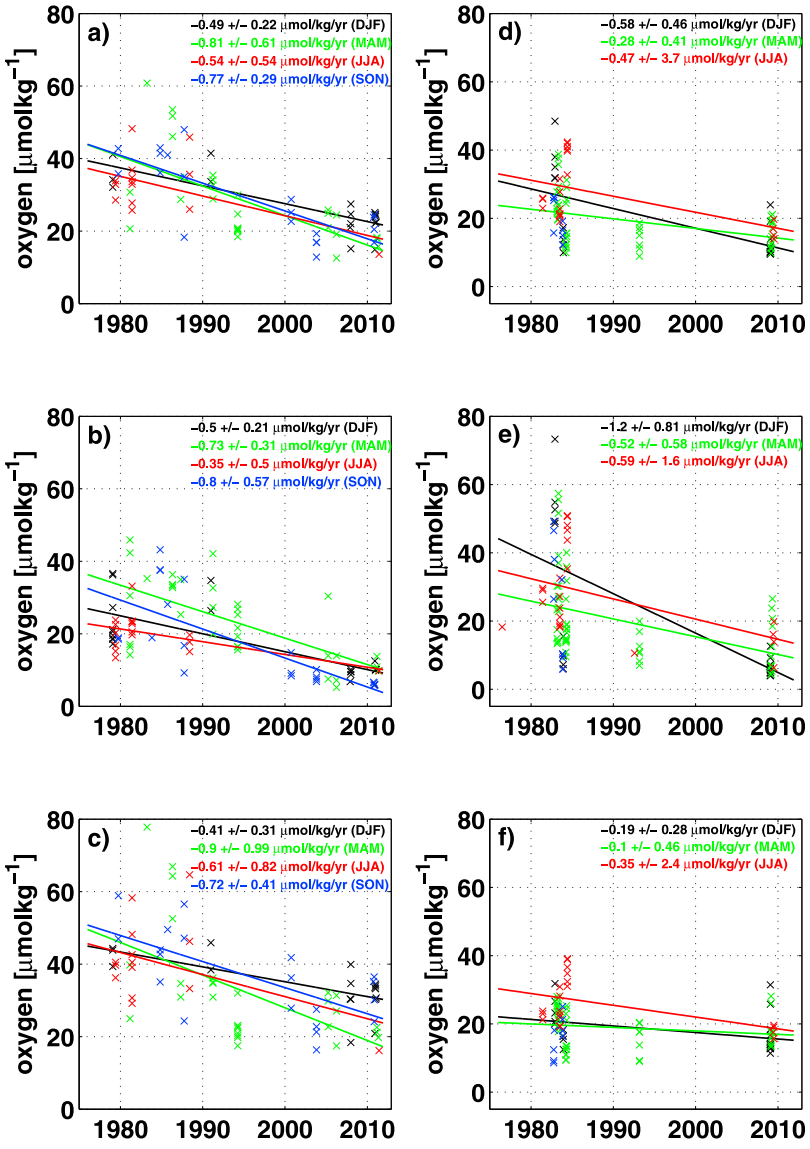

Figure 4. Time series of seasonal O_2 concentration (μmol kg^{-1}) from historical data since 1976, float data, and CTD data at float deployment locations with linear fits (solid lines) for different depth layers. Seasons are indicated by month initials, e.g., boreal winter (December, January, and February) is designated DJF. Analyzed boxes (see Figure 2) are bounded by (a–c) 5°S–2°S, 108°W–111°W and (d–f) 5°S–2°S, 84°W–87°W. Layer depths are 200–700 m (Figures 4a and 4d), 200–400 m (Figures 4b and 4e), and 400–700 m (Figures 4c and 4f). Temporal oxygen trends with 95% confidence intervals are included in each frame.

Considering a smaller area reduces the possible influence of geographic variability on estimated temporal trends and leads to a better estimate as long as the data are sufficiently numerous. For the box 3°S–3°N, 115°W–105°W, north of our box A, *Stramma et al.* [2010a] estimate a 200–700 m trend of -0.49 μmol kg^{-1} yr^{-1} since 1975. This trend reduces by 47% (to -0.23 μmol kg^{-1} yr^{-1}) when extending this computation back in time to 1960, again showing the importance of multidecadal changes for long-term trend estimation. Hence, trend estimates over a complete PDO period be more representative of long-term changes.

[22] Seasonal changes might be another source of variability. The horizontal extent, core thickness, and vertical depth range of the eastern tropical Pacific OMZ do not exhibit much of a seasonal cycle [*Paulmier and Ruiz-Pino*, 2009]. However, seasonality of the equatorial currents could influence the equatorial oxygen distribution. Therefore, we attempt to investigate the effects of any possible seasonal signal. In box B the boreal fall trend (September, October, and November: SON) cannot be derived, as no data are available since the mid-1990s in the 200–400 m layer (Figure 4e) and the mid-1980s below 400 m depth (Figure 4f). In box A (108°W–111°W, 2°S–5°S) the strongest O_2 decrease for 200 to 700 m is in spring with a trend of -0.81 ± 0.61 μmol kg^{-1} yr^{-1}, with the weakest decreasing trend of -0.49 ± 0.22 μmol kg^{-1} yr^{-1} in winter (Figure 4a). The seasonal trends for all depth ranges are all negative, of similar strength, and overlap within their respective uncertainties;

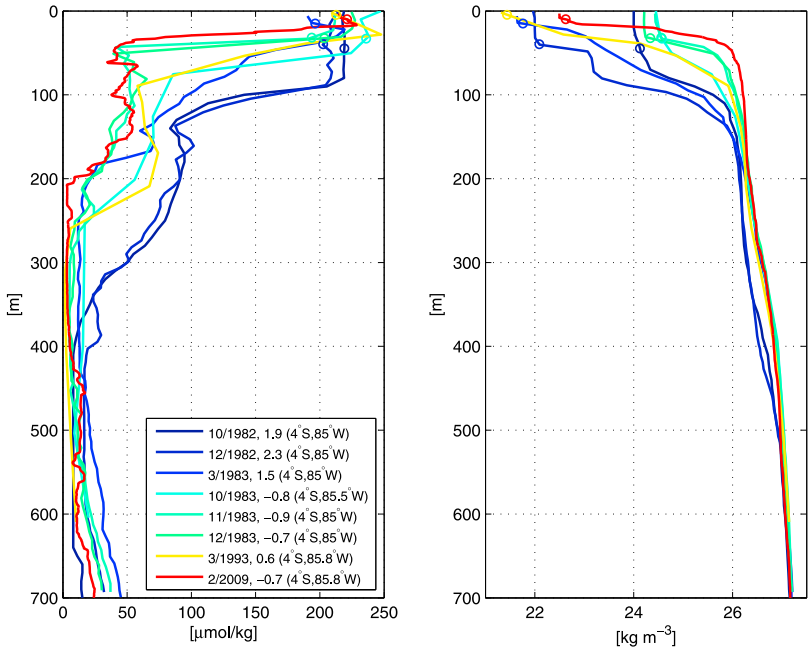

Figure 5. Profiles of (left) O_2 and (right) associated density near 4°S, 85°W during different phases of El Niño (strong are blue, weak are yellow) and La Niña (strong are blue green and red are weak). Values from a 3 month running mean Oceanic Niño Index (ONI, available at http://ggweather.com/enso/oni.htm) interpolated to section times are shown in the inset following the month and year of the shown profile. Circles indicate the mixed layer depth defined by a density difference of 0.125 kg m^{-3} compared to the surface density [*Levitus*, 1982].

hence, seasonal changes do not appear to overly influence the 200–700 m trends in box A. In box B (84°W–87°W, 2°S–5°S) the trends are of similar strength in the 200–400 m layer to those in box A, but are weaker in the 400–700 m layer for the 3 seasons available (Figure 4f). The strongest 200–700 m trend is in winter in box B, whereas it is in spring in box A. Again, both areas show decreasing oxygen for all seasons, and all seasonal trends for each layer within any given box overlap within their uncertainties.

[23] Complicating the interpretation further, on interannual time scales El Niño events modify the thickness of the OMZ. At 4°S, 85°W, El Niño dynamics modulate mixed layer depth, oxycline depth, and the vertical extent of the OMZ [*Fuenzalida et al.*, 2009]. At this location the upper 300 m of the OMZ was replaced by oxygen-rich water during El Niño in December 1982 compared to December 1983 [*Fuenzalida et al.*, 2009]. The WOCE survey of the 85°50′W section in March 1993 was made in a weak El Niño phase, while the February 2009 survey was occupied during weak La Niña conditions. A comparison of the data used here with the strong 1982 El Niño shows the strongest oxygen differences between about 50 to 150 m, mostly related to the varying mixed layer depth (Figure 5). However, the El Niño influence is visible down to about 350 m.

[24] Although the data set is small, we compare the correlation of the annual measurements with the Niño index for completeness. A comparison of the ONI 3.4 index with the detrended O_2 at the times of the monthly mean measurements in box A reveals an insignificant positive correlation ($r = 0.19$) for the upper layer of 200–400 m depth (Figure 6a), whereas the correlation is insignificant but negative ($r = -0.08$) for the lower layer of 400–700 m depth (Figure 6b). The correlation between the detrended O_2 measurements in the eastern box B and the Nino 1 + 2 index (defined for 80°W–90°W, 0°–10°S) shows an insignificant positive correlation for both depth levels, 200–400 m ($r = 0.31$) and 400–700 m ($r = 0.03$). The positive El Niño to O_2 correlations in the 200–400 m layer for both boxes, while insignificant, are consistent in sign with the variations discussed in the profiles (Figure 5). The insignificant correlations of opposite signs for the 400–700 m layer in the two boxes is consistent with the finding of negligible El Niño influence on the O_2 changes below 400 m depth and underlines the limitation of a larger El Niño influence on oxygen in the upper 400 m.

3.2. Cross-Equatorial Sections

[25] Locations with long-term time series are rare, motivating comparisons between sections. The question arises as to whether a section comparison has the ability to reproduce oxygen trends. Here we examine the changes in the eastern equatorial Pacific oxygen distribution by comparing oxygen and velocity data from the high-quality WOCE sections from the early 1990s to those from recent repeat surveys (Figure 7). Eastward relatively oxygen-rich currents supply oxygen to the OMZ while westward currents export oxygen-poor water, so it is worth checking whether a clear relation between oxygen fluxes and oxygen changes exists. On the 110°W section, low oxygen concentrations are observed from 100 to 700 m depth and between 5°S and 10°N, with the strongest minimum (concentrations <4 μmol kg^{-1}) at 500–700 m north of 8°N (Figures 7a and 7b). Relatively high oxygen values of 20–40 μmol kg^{-1} are observed in the equatorial channel between 2°S and 2°N (Figures 7a and 7b). This higher oxygen

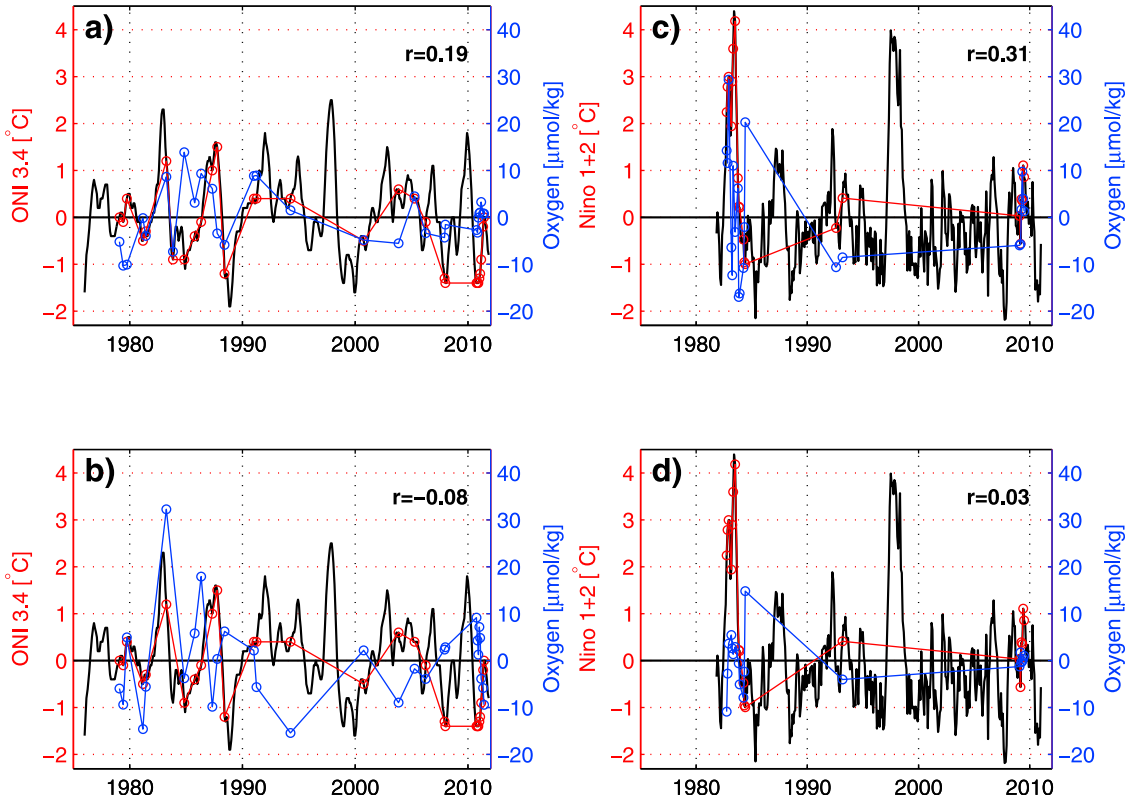

Figure 6. Detrended time series of monthly mean O_2 concentration (blue circles and blue lines) for layer depths 200–400 m in (a) box A and (c) box B and 400–700 m in (b) box A and (d) box B. ONI 3.4 (Figures 6a and 6b) and Nino 1 + 2 (Figures 6c and 6d) indices (black line). Red circles and lines mark the ONI 3.4 and Nino 1 + 2 indices at the times of the monthly mean measurements. The corresponding correlation coefficient r is included in each frame.

is clearly related to the EUC carrying relatively oxygenated water eastward. The near-zero velocity at 400 m depth on the equator, below the EUC, may contribute to a local vertical oxygen minimum there (Figure 7b).

[26] Oxygen flux divergences contribute directly to changes in oxygen concentration. Divergence can be estimated from velocity sections, but a very large number are required for a reliable estimate [*Johnson et al.*, 2001b]. Oxygen data have not been measured routinely on most cross-equatorial sections, and estimating oxygen flux divergences would not be prudent with only the pairs of sections we analyze here at 110°W and 86°W. Nonetheless, velocity changes in zonal currents, while not the entire divergence, may be related changes in oxygen concentration. With this caveat in mind, we investigate if oxygen changes are related to velocity changes along 110°W (Figure 7c, black contours). Oxygen concentrations are generally lower for 100–400 m, and even down to 600 m north of the equator in late 2007 compared with 1994, independent of any velocity differences (Figure 7c, colors). The only exception to this pattern below about 100 m depth is a region with an oxygen increase from 5°N to 7°N. The velocity difference at these latitudes shows increased eastward velocities of the NECC and the deeper NSCC, consistent with these stronger currents carrying oxygen-richer waters into the region. Aside from this band, the oxygen-poor layer extends further into the upper ocean in December 2007 (Figure 7b) leading to reduced oxygen values from 50 to 650 m in the north (Figure 7c). In December 2007 the eastward flowing EUC was weaker and associated with lower oxygen values than in April 1994. The stronger EUC in April than in December is in agreement with the observed [*Johnson et al.*, 2002] and modeled [*Cravatte et al.*, 2007] seasonal EUC transport signal at 110°W. The westward flowing SEC and the SEIC between 2°S and 4°S, which export oxygen-poor water from the OMZ, are quite strong in 1994 compared with 2007 (Figures 7a and 7b). While in the upper ocean the weaker SEC in 2007 is associated with reduced oxygen values (Figure 7c), the weaker 2007 SEIC is accompanied by enhanced oxygen values below 400 m. The time series for the 400–700 m layer reveals an oxygen value far below the trend line in 1994 (Figure 3c), putting the increase of oxygen below 400 m depth between the measurements along the 110°W section in 1994 and 2007 into context. The comparison with the long-term trend shows that an analysis of changes between two sections well separated in time may be aliased by short-term variability. Deviations from the trend might be limited vertically (as seen in Figures 3b and 3c) as well as horizontally. For example, oxygen differences between 2°S and 5°N show an overall decrease of oxygen below 400 m (Figure 7c) and different from the 5°S to 2°S region might reproduce a long-term decrease for this region. At 110°W the December 2007 cruise was during a La Niña phase and should be relatively oxygen-poor in the upper ocean compared to April 1994. In the 110°W

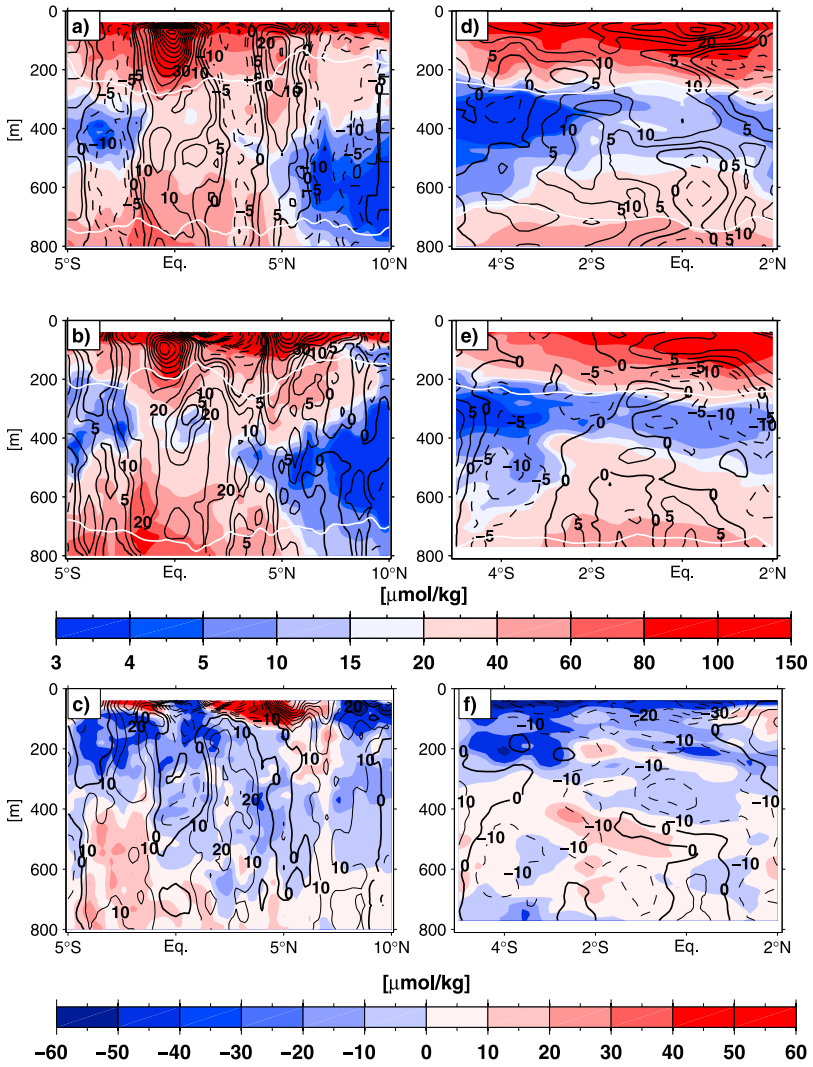

Figure 7. Distributions of O_2 (color, μmol kg^{-1}) and ADCP-measured zonal velocity (black contours, cm s^{-1}, positive eastward) versus depth and latitude along 110°W (a) in April 1994 and (b) in December 2007 to January 2008 and (c) differences in oxygen (color, μmol kg^{-1}) and velocity (black contours, cm s^{-1}, positive stronger eastward component in 2007) between the December 2007 to January 2008 cruise and the April 1994 cruise. Distributions of O_2 (color, μmol kg^{-1}) and ADCP-measured zonal velocity (black contours, cm s^{-1}, positive eastward) along 85°50′W (d) in March–April 1993, (e) in February 2009 and (f) differences in oxygen (color, μmol kg^{-1}) and velocity (black contours, cm s^{-1}, positive stronger eastward component in 2009) between the February 2009 cruise and the March–April 1993 cruise. Depths of isopycnals 26.4 kg m^{-3} (shallow) and 27.2 kg m^{-3} (deep) are overlaid (white lines).

sections the OMZ expands vertically with time, especially below the mixed layer. In contrast, expansion below the mixed layer is not obvious at 85°50′W. At 110°W, modeling results [*Cravatte et al.*, 2007] show much stronger upwelling in December than in April; hence, the upward expansion of the low oxygen layer at 110°W (Figures 7c) might be caused by seasonal strengthening of upwelling. As described before, the seasonal signal would lead to a stronger EUC with higher oxygen supply, and the different signals cannot be separated with only two sections available.

[27] At 85°50′W our analysis is limited to between 5°S and 2°N, where deep velocity measurements exist for both cruises (Figures 7d–7f). In large parts of the upper 300 to 400 m the oxygen at 85°50′W decreases, while between ~300–400 and 700 m oxygen increases cover a larger cross-section than decreases. Typical for El Niño conditions, in March 1993 the eastward flow was stronger and oxygen concentrations higher in the upper 200 m than in February 2009 (Figures 7d–7f), while no clear El Niño signal can be assigned to the deeper part of the OMZ, in agreement with the results described before (Figures 5 and 6). The EUC was much stronger in March 1993 (Figure 7d) than in February 2009 (Figure 7e) and is associated with reduced oxygen concentrations with time (Figure 7f), likely due to a reduced supply of oxygenated water. Below the EUC at 500–700 m depth the westward flow at 0° to 1°N in March 1993 is probably a weak EIC. In 2009 a strong EIC is observed between 1°S and 2°N and 200–400 m depth, perhaps causing a stronger westward

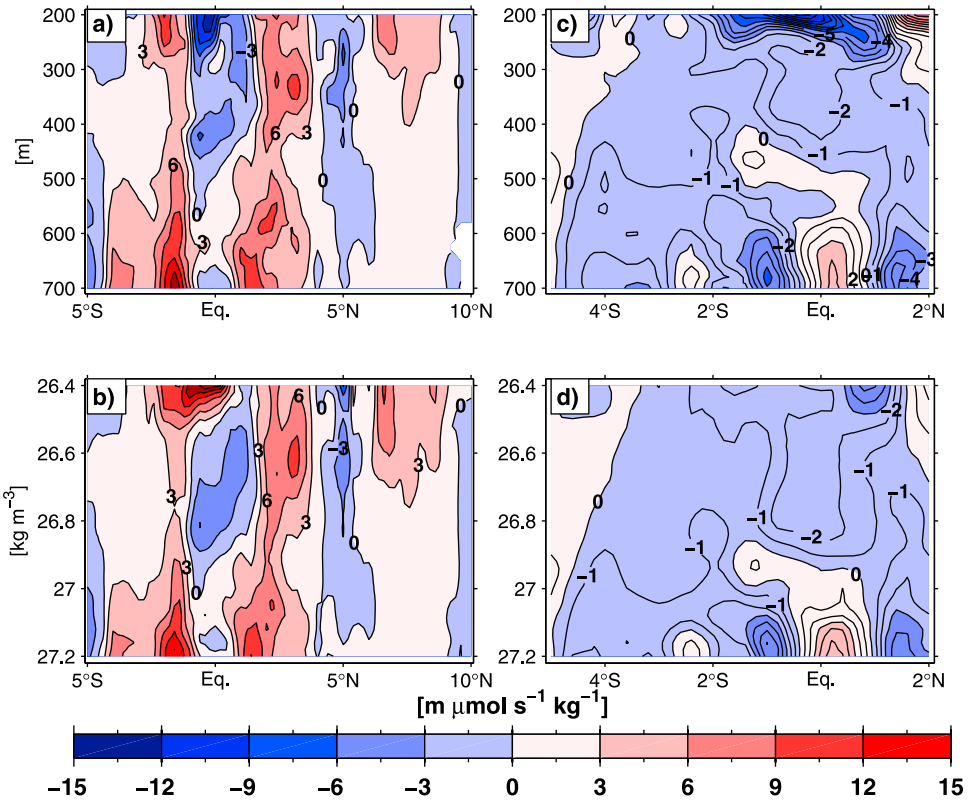

Figure 8. Oxygen flux differences (color, m μmol s^{-1} kg^{-1}) versus latitude and depth (a) along 110°W between December 2007 to January 2008 and April 1994 and (c) along 85°50′W between February 2009 and March–April 1993. The oxygen flux differences versus latitude and density are also shown (b) for 110°W and (d) for 85°50′W. Depth locations of the upper and lower isopycnals in Figures 8b and 8d are marked in Figure 7. Contour line spacings differ for 110°W and 85°50′W, but the color scale is the same.

transport of oxygen-poor water from the OMZ (Figure 7e) and a decrease in oxygen around the equator at about 400 m depth (Figure 7f). The northern part of the eastward flowing SSCC is clearly visible south of 4.5°S in February 2009. As there was no discernible SSCC in March 1993 the flow difference for February 2009 is eastward and, at least below 300 m, the oxygen increase could be related to the increased supply of oxygen-richer water from the west in 2009. The 2009 section shows a westward SEIC between 4.5°S and 3°S with a strong velocity core at about 500 m depth (Figure 7e). The local oxygen minimum core at 3.5°S in 500–600 m depth (Figure 7f) is associated with the stronger westward transport of deoxygenated water from the OMZ in 2009. Similar to 110°W, some oxygen changes appear related to velocity changes, especially in the equatorial channel. The accord between signs of zonal current and oxygen changes due to the negative zonal oxygen gradient is only found in slightly over 50% of the overall cross-sectional area considered for each section. The annual mean in 1993 for the layer between 400 and 700 m (Figure 3f) is based only on the R/V *Knorr* section from February to April and shows an oxygen value below the overall trend line, again putting the slight oxygen increase along the 85°50′W sections between 1993 and 2009 below 400 m depth into context.

[28] Oxygen changes on depth surfaces can be owing to changes on density surfaces and vertical motions (heave) of density surfaces. Isopycnal heave can occur over very short time scales, owing to the influence of internal waves, internal tides, planetary waves, and eddies. The differences in oxygen versus density for $\sigma_\theta \geq 25.5$ kg m^{-3} strongly resembles the differences in oxygen versus depth (Figures 7c and 7f); hence, isopycnal heave does not have a strong influence on oxygen differences in these particular sections. Overall, oxygen changes versus depth and versus density are largely similar, in agreement with a recent result that most of the zonally averaged pattern of oxygen change is associated with oxygen changes on density surfaces [*Helm et al.*, 2011].

[29] The correlations between the oxygen and temperature differences are 51.3% at 110°W and 49.9% for 85°50′W. Hence, as for the time series since 1975, there is no relation between temperature and oxygen changes.

[30] The differences in section oxygen fluxes ($u \cdot O_2$) along 110°W between December 2007 and April 1994 (Figure 8a) resemble the velocity differences (Figure 7c), however the oxygen fluxes clearly show the loss or gain in oxygen related to the velocity distribution. The oxygen fluxes versus density between 26.4 and 27.2 kg m^{-3} (isopycnals shown in Figures 7a and 7b), a density range chosen to roughly cover the 200–700 m layer, show a quite similar distribution as versus depth. The larger positive oxygen flux between 2°S and the equator of between 26.4 and 26.5 kg m^{-3} (Figure 8a) is caused by the different depths of the isopycnals in the EUC (Figures 7a and 7b). In 1994 the isopycnal 26.4 kg m^{-3} was up to 100 m deeper than in 2007. The oxygen flux differences at 85°50′W

(Figures 8c and 8d) show mainly lower eastward fluxes in February 2009 compared to March 1993. However, the oxygen flux differences are weak when compared to 110°W, owing to the general weaker current velocities at 85°50′W. The weakness is in part caused by the topographic barrier of the Galapagos Islands near the equator at about 90°W–92°W.

[31] The oxygen flux differences are not sufficient to explain the observed O_2 trends. The increase at 110°W in the layer 400–700 m between 5°S and 2°S (Figure 3c) are well related to the positive oxygen flux differences in the same area (Figure 8a), however the O_2 increase at 85°50′W at 5°S to 2°S for the 400–700 m layer is in a region of negative oxygen flux differences (Figure 8d). Hence, a comparison between oxygen fluxes of two sections might lead to inferences about oxygen changes differing from the actual long-term trends. In addition to the issue of transport versus divergence of transport, variability probably occurs on a variety of time scales, which is not captured by comparing two discrete occupations some years apart.

4. Discussion and Summary

[32] Our investigation shows overall reductions in oxygen content in the eastern equatorial Pacific OMZ over the last few decades, with variations at multiple time scales superimposed. The variance explained by linear trends in dissolved oxygen concentration in the depth layers considered here is between 26% and 78% for the two boxes investigated (Table 2). The only two variance values below 55% were for the deepest, 400–700 m, layer in each box. Variability on shorter time scales or larger spatial scales may influence or alias the linear trends computed here. For instance, off California the observed oxygen changes over the last 57 years have not been monotonic, with earlier decreases reversing in the mid-1980s, bringing recent concentrations back up to levels measured in the late 1950s to early 1960s [*McClatchie et al.*, 2010]. Temperature trends are not significant in the 200–700 m layers, nevertheless the comparison between oxygen and temperature changes shows that the oxygen trends in the long time series as well as for the differences between two sections are not easily linked to temperature-driven changes in oxygen solubility.

[33] Our results indicate a large influence of the PDO index on oxygen changes. In a model analysis [*Deutsch et al.*, 2011] such changes are associated with variations in the depth of the tropical and subtropical thermocline. In this model, decadal changes in respiration, driven by circulation changes, modulate the tropical Pacific OMZ. Hence, OMZ changes mirror, but in an amplified way, vertical excursions of the eastern thermocline associated with changes in the PDO index. Our comparisons of O_2 trends for periods starting at 1960 and at 1976 suggest that the PDO has a large influence on the trends, enhancing by more than 200% for the period starting in 1976 versus that starting in 1960. These changes may be linked to observed decadal variability of the shallow Pacific meridional overturning circulation, with a trend toward a decrease in equatorial convergence from 1970 to the mid-1990s [*Zhang and McPhaden*, 2006] which should lead to a reduced equatorial circulation. This trend has reversed since the mid-1990s [*Schott et al.*, 2008]. The reversal could be related to a weakening in the trend of the eastern equatorial Pacific OMZ increase since the 1990s in most depths of the two boxes analyzed here (Figure 3). However, the trends since 1993 at 110°W are not statistically significant mainly due to the excursion to low oxygen in 1994 and at 85°50′W there are only 2 years of data during this time period.

[34] We also investigate other sources of oxygen variability. As the equatorial eastward currents carry slightly oxygen-richer water eastward toward the OMZ [*Stramma et al.*, 2010a], some oxygen variability could be related to variations in velocity. However, the influence of advection variability is apparently weak. Oxygen time series south of the equator covering the westward current bands exporting oxygen-poor water from the OMZs at about 110°W and 85°50′W yield decreases in trends of oxygen concentration for 200–700 m of -0.83 μmol kg^{-1} yr^{-1} and -0.50 μmol kg^{-1} yr^{-1}, respectively, over the last 34 years. Well-calibrated O_2 profiles from floats are useful in augmenting these time series in recent years. At 110°W the trend of -0.83 μmol kg^{-1} yr^{-1} south of the equator is higher than a previously described decreasing trend of -0.49 μmol kg^{-1} yr^{-1} [*Stramma et al.*, 2010a] centered on the equator. The equatorial box in that study covered a much larger area (105°W–115°W, 3°S–3°N) including some lateral oxygen gradients. These gradients may have aliased the trend estimate. However, the trend computations for the box 105°W–115°W, 5°S–5°N [*Stramma et al.*, 2008] also show a strong dependence of the trend of the time period investigated, probably caused by the PDO.

[35] A comparison of repeated hydrographic sections at 110°W (1994 and 2007) and 85°50′W (1993 and 2009) shows that at some locations, especially near the equator, enhanced oxygen is related to stronger eastward flow; however, this result is not general, as countervailing regions are found. Similarly, the oxygen fluxes related to the velocity field cannot explain the observed oxygen changes at all locations. The decreasing trend seems to be in part a long-term OMZ change with some variability superimposed that could be related to decadal climate and circulation oscillations [*Deutsch et al.*, 2011; *Zhang and McPhaden*, 2006]. El Niño influences are also visible in the 200–400 m layer O_2 time series and in the upper 350 m of the 85°50′W section, but no clear influence is apparent below this depth. The O_2 changes versus density are very similar to the changes versus depth; hence, the influence of isopycnal heave is small for the sections compared.

[36] The continuous time series reveal that comparing only two sections may lead to erroneous conclusions, especially if El Niño events or decadal variations modify the upper ocean oxygen distributions during their occupation. The trends between the two section pairs for the layer of 400–700 m depth within the range of the boxes used for the trend computations are positive at 110°W and negligible at 85°50′W (Figure 3, dashed lines), while the long-term trend reveals a significant oxygen decrease. Trend computations for the western box since 1993 lead to a weakened negative trend for the 200–700 m layer, but the uncertainties are large, and hence, it is not possible to prove a weakened oxygen decrease since the early 1990s with the present data set. In the future floats with oxygen sensors might play an important role in allowing construction of nearly continuous time series in regions with sparse or infrequent ship-based hydrographic surveys.

[37] The comparison of trend computations with the results from section differences reveals that a comparison of sections could be done if no time series can be constructed; however, influences of seasonal and longer-term signals can obscure such a comparison. Hence, the differences observed have to be interpreted with caution. Our analysis further reveals the causes for anomalous points in the time series and suggests that variations might be different for a time series at a neighboring location. Our results from the comparison of long-term trends with variability on shorter time scales and our analyses of the repeat sections can be used to understand better the influence of physical processes including zonal current bands, variations in horizontal fluxes, and isopycnal heave as well as climate variations such as the seasonal cycle, El Niño, and the Pacific Decadal Oscillation on the calculated oxygen trends.

[38] **Acknowledgments.** Financial support was received through the GEOMAR (R.C. and L.S.) and the NOAA Office of Ocean and Atmospheric Research (G.C.J.). This work is a contribution of the DFG-supported project SFB754 (http://www.sfb754.de/) which is supported by the Deutsche Forschungsgemeinschaft. Findings and conclusions in this article are those of the authors and do not necessarily represent the views of the National Oceanic and Atmospheric Administration. PMEL publication 3759.

References

Bopp, L., C. Le Quere, M. Heimann, A. C. Manning, and P. Monfray (2002), Climate induced oceanic oxygen fluxes: Implications for the contemporary carbon budget, *Global Biogeochem. Cycles*, *16*(2), 1022, doi:10.1029/2001GB001445.

Boyer, T. P., J. I. Antonov, H. E. Garcia, D. R. Johnson, R. A. Locarnini, A. V. Mishonov, M. T. Pitcher, O. K. Baranova, and I. V. Smolyar (2006), *World Ocean Database 2005*, *NOAA Atlas NESDIS*, vol. 60, edited by S. Levitus, 190 pp., U.S. Gov. Print. Off., Washington, D. C.

Chavez, F. P., J. Ryan, S. E. Lluch-Cota, and M. Niquen (2003), From anchovies to sardines and back: Multidecadal change in the Pacific Ocean, *Science*, *299*, 217–221, doi:10.1126/science.1075880.

Cravatte, S., G. Madec, T. Izumo, C. Menkes, and A. Bozec (2007), Progress in the 3-D circulation of the eastern equatorial Pacific in a climate ocean model, *Ocean Modell.*, *17*, 28–48, doi:10.1016/j.ocemod.2006.11.003.

Curry, R. (2008), HydroBase2, http://www.whoi.edu/PO/hydrobase/, Woods Hole Oceanogr. Inst., Woods Hole, Mass.

Czeschel, R., L. Stramma, F. U. Schwarzkopf, B. S. Giese, A. Funk, and J. Karstensen (2011), Middepth circulation of the eastern tropical South Pacific and its link to the oxygen minimum zone, *J. Geophys. Res.*, *116*, C01015, doi:10.1029/2010JC006565.

Deser, C., M. A. Alexander, S.-P. Xie, and A. S. Phillips (2010), Sea surface temperature variability: Patterns and mechanisms, *Annu. Rev. Mar. Sci.*, *2*(1), 115–143, doi:10.1146/annurev-marine-120408-151453.

Deutsch, C., S. Emmerson, and L. Thompson (2006), Physical-biological interactions in North Pacific oxygen variability, *J. Geophys. Res.*, *111*, C09S90, doi:10.1029/2005JC003179.

Deutsch, C., H. Brix, T. Ito, H. Frenzel, and L. Thompson (2011), Climate-forced variability of ocean hypoxia, *Science*, *333*, 336–339, doi:10.1126/science.1202422.

Eden, C., and A. Timmermann (2004), The influence of the Galapagos Islands on the tropical temperatures, currents and the generation of tropical instability waves, *Geophys. Res. Lett.*, *31*, L15308, doi:10.1029/2004GL020060.

Firing, E., S. E. Wijffels, and P. Hacker (1998), Equatorial subthermocline currents across the Pacific, *J. Geophys. Res.*, *103*, 21,413–21,423, doi:10.1029/98JC01944.

Fuenzalida, R., W. Schneider, J. Garces-Vargas, L. Bravo, and C. Lange (2009), Vertical and horizontal extension of the oxygen minimum zone in the eastern South Pacific Ocean, *Deep Sea Res., Part II*, *56*, 992–1003, doi:10.1016/j.dsr2.2008.11.001.

Gnanadesikan, A., J. P. Dunne, and J. John (2012), Understanding why the volume of suboxic waters does not increase over centuries of global warming in an Earth System Model, *Biogeosciences*, *9*, 1159–1172, doi:10.5194/bg-9-1159-2012.

Helm, K. P., N. L. Bindoff, and J. A. Church (2011), Observed decreases in oxygen content of the global ocean, *Geophys. Res. Lett.*, *38*, L23602, doi:10.1029/2011GL049513.

Johnson, G. C., P. E. Robbins, and G. E. Hufford (2001a), Systematic adjustments of hydrographic sections for internal consistency, *J. Atmos. Oceanic Technol.*, *18*, 1234–1244, doi:10.1175/1520-0426(2001)018<1234:SAOHSF>2.0.CO;2.

Johnson, G. C., M. McPhaden, and E. Firing (2001b), Equatorial Pacific ocean horizontal velocity, divergence, and upwelling, *J. Phys. Oceanogr.*, *31*, 839–849, doi:10.1175/1520-0485(2001)031<0839:EPOHVD>2.0.CO;2.

Johnson, G. C., B. M. Sloyan, W. S. Kessler, and K. E. McTaggart (2002), Direct measurements of upper ocean currents and water properties across the tropical Pacific during the 1990's, *Prog. Oceanogr.*, *52*, 31–61, doi:10.1016/S0079-6611(02)00021-6.

Karnauskas, K. B., R. Murtugudde, and A. J. Busalacchi (2007), The effect of the Galapagos Islands on the equatorial Pacific cold tongue, *J. Phys. Oceanogr.*, *37*, 1266–1281, doi:10.1175/JPO3048.1.

Karnauskas, K. B., R. Murtugudde, and A. J. Busalacchi (2010), Observing the Galapagos-EUC interaction: Insights and challenges, *J. Phys. Oceanogr.*, *40*, 2768–2777, doi:10.1175/2010JPO4461.1.

Karstensen, J., L. Stramma, and M. Visbeck (2008), Oxygen minimum zones in the eastern tropical Atlantic and Pacific Oceans, *Prog. Oceanogr.*, *77*, 331–350, doi:10.1016/j.pocean.2007.05.009.

Kessler, W. S. (2006), The circulation of the eastern tropical Pacific: A review, *Prog. Oceanogr.*, *69*, 181–217, doi:10.1016/j.pocean.2006.03.009.

Knauss, J. A. (1966), Further measurements and observations on the Cromwell Current, *J. Mar. Res.*, *24*, 205–240.

Levitus, S. (1982), *Climatological Atlas of the World Ocean*, *NOAA/ERL GFDL Prof. Pap. 13*, 173 pp., Geophys. Fluid Dyn. Lab., Princeton, N. J.

Matear, R. J., and C. Hirst (2003), Long-term changes in dissolved oxygen concentrations in the ocean caused by protracted global warming, *Global Biogeochem. Cycles*, *17*(4), 1125, doi:10.1029/2002GB001997.

McClatchie, S., R. Goericke, R. Cosgrove, G. Auad, and R. Vetter (2010), Oxygen in the Southern California Bight: Multidecadal trends and implications for demersal fisheries, *Geophys. Res. Lett.*, *37*, L19602, doi:10.1029/2010GL044497.

Oschlies, A., K. G. Schulz, U. Riebesell, and A. Schmittner (2008), Simulated 21st century's increase in oceanic suboxia by CO_2-enhanced biotic carbon export, *Global Biogeochem. Cycles*, *22*, GB4008, doi:10.1029/2007GB003147.

Pak, K., and J. R. V. Zaneveld (1973), The Cromwell Current on the east side of the Galapagos Islands, *J. Geophys. Res.*, *78*, 7845–7859, doi:10.1029/JC078i033p07845.

Paulmier, A., and D. Ruiz-Pino (2009), Oxygen minimum zones (OMZs) in the modern ocean, *Prog. Oceanogr.*, *80*, 113–128, doi:10.1016/j.pocean.2008.08.001.

Prince, E. D., and C. P. Goodyear (2006), Hypoxia-based habitat compression of tropical pelagic fishes, *Fish. Oceanogr.*, *15*, 451–464, doi:10.1111/j.1365-2419.2005.00393.x.

Rowe, G. D., E. Firing, and G. C. Johnson (2000), Pacific equatorial subsurface countercurrent velocity, transport, and potential vorticity, *J. Phys. Oceanogr.*, *30*, 1172–1187, doi:10.1175/1520-0485(2000)030<1172:PESCVT>2.0.CO;2.

Schott, F. A., L. Stramma, W. Wang, B. S. Giese, and R. Zantopp (2008), Pacific subtropical cell variability in the SODA 2.0.2/3 assimilation, *Geophys. Res. Lett.*, *35*, L10607, doi:10.1029/2008GL033757.

Stramma, L., G. C. Johnson, J. Sprintall, and V. Mohrholz (2008), Expanding oxygen-minimum zones in the tropical oceans, *Science*, *320*, 655–658, doi:10.1126/science.1153847.

Stramma, L., G. C. Johnson, E. Firing, and S. Schmidtko (2010a), Eastern Pacific oxygen minimum zones: Supply paths and multidecadal changes, *J. Geophys. Res.*, *115*, C09011, doi:10.1029/2009JC005976.

Stramma, L., S. Schmidtko, L. A. Levin, and G. C. Johnson (2010b), Ocean oxygen minima expansions and their biological impacts, *Deep Sea Res., Part I*, *57*, 587–595, doi:10.1016/j.dsr.2010.01.005.

Tsuchiya, M. (1975), Subsurface countercurrents in the eastern equatorial Pacific Ocean, *J. Mar. Res.*, *33*, Suppl., 145–175.

Tsuchiya, M., and L. D. Talley (1998), A Pacific hydrographic section at 88°W: Water-property distribution, *J. Geophys. Res.*, *103*, 12,899–12,918, doi:10.1029/97JC03415.

von Storch, H., and F. W. Zwiers (1999), The decorrelation time, in *Statistical Analysis in Climate Research*, pp. 371–374, Cambridge Univ. Press, Cambridge, U. K.

Wunsch, C. (1996), Least squares, in *The Ocean Circulation Inverse Problem*, pp. 113–119, Cambridge Univ. Press, Cambridge, U. K., doi:10.1017/CBO9780511629570.

Zhang, D., and M. J. McPhaden (2006), Decadal variability of the shallow Pacific meridional overturning circulation: Relation to tropical sea surface temperatures in observations and climate change models, *Ocean Modell.*, *15*, 250–273, doi:10.1016/j.ocemod.2005.12.005.